FERMILAB-CONF-07-737-E

Recent CDF Results

Gervasio Gómez
(for the CDF Collaboration)

Instituto de Física de Cantabria
Av. Los Castros s/n, 39005 Santander, Spain.

Abstract. As of November of 2007, the CDF detector has recorded approximately 2.7 fb^{-1} of data. This contribution describes some of the most recent and most relevant results from the CDF collaboration in all areas of its wide physics program, as well as some insights into the Tevatron reach for Higgs searches within the next few years.

Keywords: experimental high energy physics, hadron collider physics
PACS: 10

INTRODUCTION

The physics program of the CDF collaboration includes the study of jet production, heavy flavor production, electroweak and top physics, as well as searches for Higgs and manifestations of physics beyond the Standard Model (SM). These processes have production cross sections which span over nine orders of magnitude, from about 10^9 pb for inclusive jet production, to the smallest cross sections ever measured at hadron colliders, of the order of 1 pb, for WZ, single top, ZZ and Higgs production. Run 2 of the Tevatron started in March of 2001, after a significant upgrade of the detector [1]. Since then, CDF has published over 140 articles, with 45 publications in 2006, 30 (expect to reach $\sim$ 40) in 2007, and over 50 publications which are still under internal review. Some of the CDF physics highlights from Run 2 include: observation of B_s mixing, $D^0 - \bar{D}^0$ (charm) mixing and new baryon states, the single most precise top mass, W mass and W width measurements, observation of WZ and ZZ production, stringent limits on anomalous triple gauge couplings, evidence for single top production, significant exclusion or reach in several beyond SM models, and constant sensitivity improvements in Higgs searches. This contribution focuses on some of the results, organized by physics topic according to the following outline:

- QCD
  - Inclusive and dijet cross section
- Heavy Flavor
  - B_s oscillations
  - B_s lifetime, $\Delta\Gamma_s$
  - $B_s \to \mu^+\mu^-$
  - Charm mixing ($D^0 - \bar{D}^0$)
- Electroweak
  - M_W and Γ_W

  - WZ and ZZ
- Top
  - M_t
  - $t\bar{t}$ cross section
  - Single top
- Higgs Search
  - Standard Model Higgs
  - MSSM Higgs
- Beyond SM Searches
  - SUSY
  - Extra dimensions + gravitons
  - Heavy resonances

QCD

The study of jet production at hadron colliders provides an important test of perturbative QCD (pQCD) predictions, with a cross section which spans over eight orders of magnitude as a function of jet p_T. The high p_T tail probes distances down to $\sim 10^{-19}$ m and is sensitive to new physics (such as quark compositeness), and the measurement of the differential cross section as a function of p_T and rapidity can be used to constrain the PDFs at high x and Q^2, particularly the gluon PDFs which are poorly known in this kinematic region.

Inclusive Jet Cross Section

From a data sample with an integrated luminosity of 1.13 fb^{-1}, inclusive jet events are selected by requiring at least one jet with $p_T > 20$ GeV/c and rapidity $|y| < 2.1$. Jets are reconstructed using the Midpoint jet clustering algorithm [2] with cone radius $R = 0.7$ and merge fraction $f_{\text{merge}} = 0.75$, and their energy is corrected for detector effects down to the hadron and parton levels. The inclusive differential jet cross section is split into five rapidity regions based on detector geometry: $|y| < 0.1$, $0.1 < |y| < 0.7$, $0.7 < |y| < 1.1$,$1.1 < |y| < 1.6$ and $1.6 < |y| < 2.1$. Figure 1 shows the measured and the predicted differential inclusive jet cross section as a function of jet p_T. Good agreement with NLO pQCD predictions is observed in all the jet rapidity regions. The figure also shows the data/theory ratio. The overall experimental uncertainty in the forward-most rapidity region is smaller than the PDF uncertainty, so this measurement can be useful to constrain global PDF fits.

Di-jet Cross Section

Using the same data sample and the same jet clustering algorithm described above, events are selected with at least two central, energetic jets. Each jet must satisfy $p_T > 20$

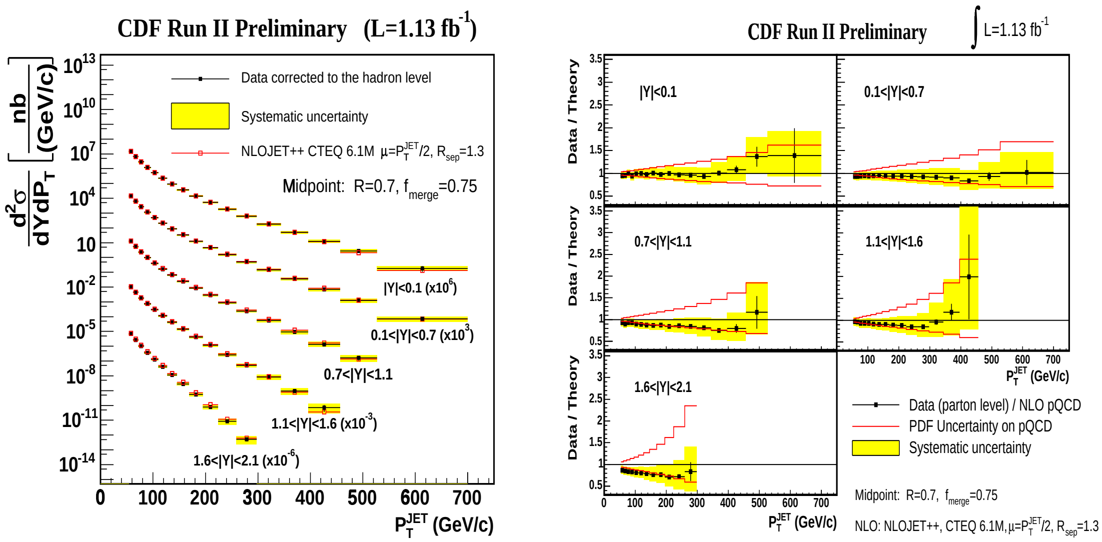

FIGURE 1. Left: The solid points and lines are the measured differential inclusive jet cross sections as a function of p_T for the different rapidity regions. The dashed points and lines represent NLO pQCD predictions. Right: data/theory differential cross section ratio.

GeV/c and $|y| < 1.0$, and only events with a dijet invariant mass $m_{jj} > 180$ GeV/c^2 are considered. Figure 2 shows the measured differential cross section as a function of invariant dijet mass, together with NLO pQCD predictions, as well as the data/theory ratio. Good agreement is found with theoretical predictions in the entire dijet mass range.

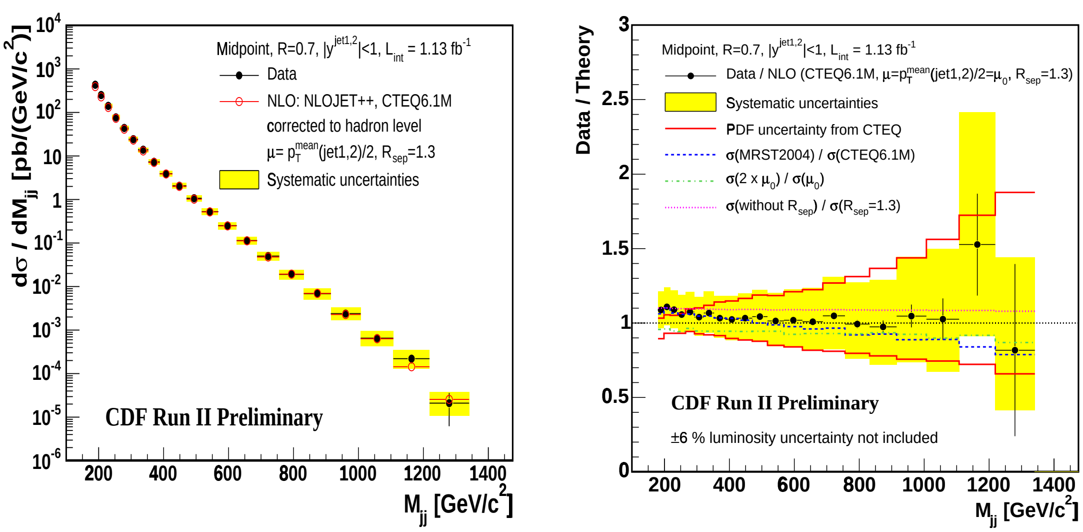

FIGURE 2. Left: The solid points and lines are the measured differential inclusive jet cross sections as a function of p_T for the different rapidity regions. The dashed points and lines represent NLO pQCD predictions. Right: data/theory differential cross section ratio.

HEAVY FLAVOR PHYSICS

The study of heavy flavor at the Tevatron has the advantage that the $b\bar{b}$ and $c\bar{c}$ cross sections are large and that all b and c hadron species are produced thanks to the large center of mass energy available. However, the overall inelastic $p\bar{p}$ cross section is very large and events are typically very busy, resulting in very large backgrounds. This makes it necessary to use triggers specifically designed to select heavy flavor events, following two basic strategies:

Lepton triggers (μ, e): select semileptonic and leptonic decays of b and c hadrons providing a clean signature in a hadronic environment where most tracks are pions.

Displaced track triggers: Select decays of B and D mesons which have long lifetimes. Requires very fast track and impact parameter reconstruction in busy events, performed at CDF by the Silicon Vertex Trigger (SVT) [3].

In addition to the conventional dimuon (J/ψ) trigger and displaced track plus lepton trigger (used for semileptonic modes), the CDF-II detector has a unique two-displaced-tracks trigger which allows to trigger on fully hadronic decays.

B_s Oscillations

Oscillation of B mesons from particle to antiparticle due to flavor-changing weak interactions has been established in the B_d and B_s systems, confirming the interpretation of the observed "heavy" and "light" mass eigenstates as a superposition of the particle and antiparticle flavor states. The observation of B_s oscillation and the subsequent measurement of its frequency are among the most important results from Run 2 of the Tevatron. Together with a precise determination of the B_d oscillation frequency, the ratio of the CKM matrix elements $|V_{td}|/|V_{ts}|$ can be determined with high precision, contributing to a stringent test of the unitarity of the CKM matrix. Using 1 fb^{-1} of data, CDF triggers both on semileptonic and fully hadronic B_s decays thanks to its unique SVT trigger. The time evolution of B_s mesons that decay with the same or opposite flavor as their flavor at production is studied as a function of proper decay time, measured from the distance between production and decay points. The B_s flavor at decay is determined unambiguously from the charges of the decay products. The flavor at production is inferred from characteristics of b quark production and fragmentation in $p\bar{p}$ collisions, which give rise to several "flavor tagging" characteristics such as the charge of the lepton, kaon, or b-jet tracks in the side opposite to the trigger B_s, the charge of fragmentation kaons, and the charge of the kaons in the same side as the trigger B_s. Figure 3 shows the result of an amplitude scan of the B_s time evolution as a function of the oscillation frequency Δm_s. The amplitude of such a scan should be zero far from the true oscillation frequency, and unity close to the true frequency. The probability that the background (with no oscillation) fluctuates to give such a signal is $\sim 8x10^{-8}$, equivalent to a 5σ fluctuation. The B_s oscillation frequency is determined to be $\Delta m_s = 17.77 \pm 0.10(\text{stat}) \pm 0.07(\text{syst})$ ps^{-1}, and we determine $|V_{td}|/|V_{ts}| = 0.2060 \pm 0.0007(\text{exp})^{+0.081}_{-0.0060}(\text{theor})$, no longer limited by experimental precision.

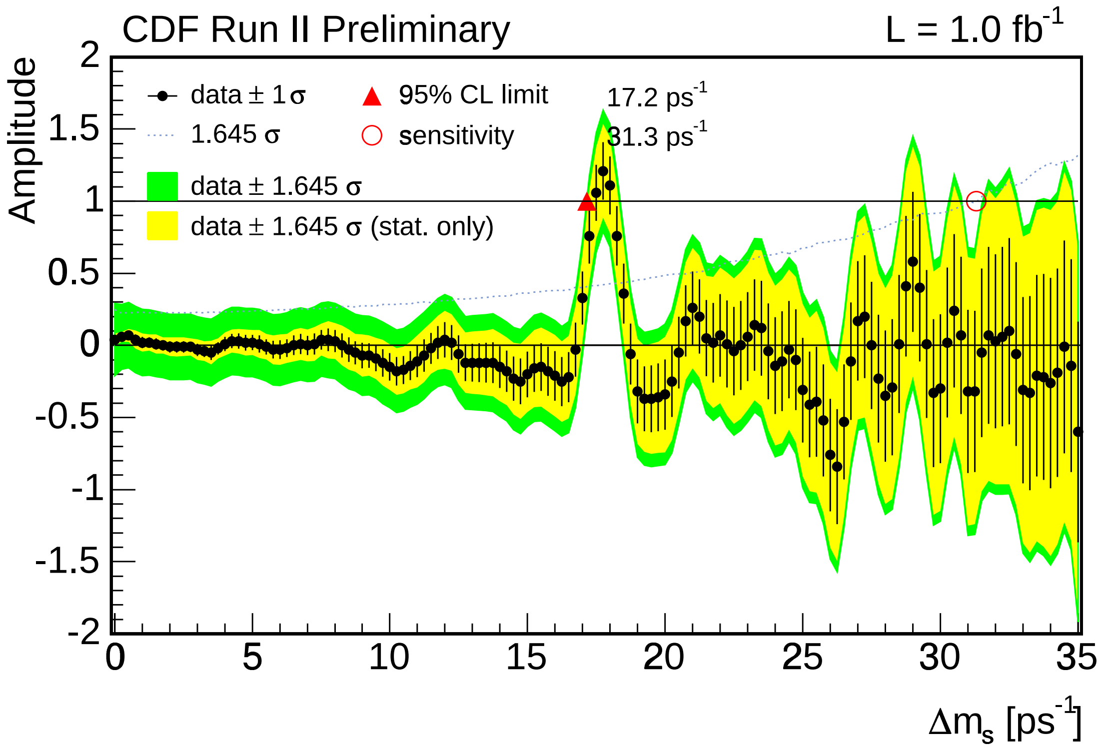

FIGURE 3. Measured amplitude values and uncertainties versus the $B_s - \bar{B_s}$ oscillation frequency Δm_s. At 17.77 ps^{-1} the amplitude is consistent with one and inconsistent with zero at 5 standard deviations.

B_s Lifetime Difference $\Delta\Gamma_s$

The mass difference between the heavy and light mass eigenstates determines the oscillation frequency of B_s mesons. Another quantity which determines the time evolution of B_s mesons is the decay rate difference $\Delta\Gamma_s = \Gamma_L - \Gamma_H$. Assuming no CP violation, the light and heavy mass eigenstates have well defined CP parity, and therefore different angular distribution of its decay products. A simultaneous fit to mass, lifetime, and angular variables in $B_s \to J/\psi\ \phi$ decays allows to separate the CP even state B_{sL} from the CP odd state B_{sH} and measure the lifetime difference. Figure 4 shows the lifetime and mass projections of such a fit. Fixing the CP violating phase $\phi_s = 0$ in the fit yields $\Delta\Gamma_s = 0.076^{+0.059}_{-0.063}(\mathrm{stat}) \pm 0.006(\mathrm{syst})\ \mathrm{ps}^{-1}$, consistent with the SM prediction of 0.096 ps^{-1}, and a mean lifetime $c\tau_s = 456 \pm 13(\mathrm{stat}) \pm 7(\mathrm{syst})\mu\mathrm{m}$.

$B_s/B_d \to \mu\mu$

In the SM, the flavor changing neutral current (FCNC) decays $B_s/B_d \to \mu^+\mu^-$ proceed through loop diagrams such as the one shown in figure 5 (top-left) and are heavily suppressed. The SM predicts the branching ratios (BR) $\mathrm{BR}(\mathrm{B_s} \to \mu^+\mu^-) =$

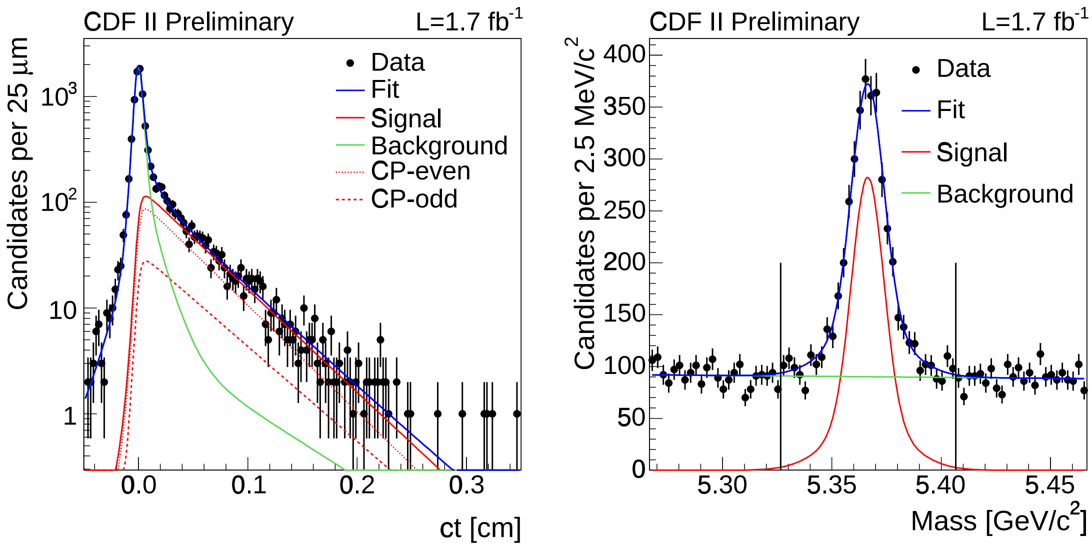

FIGURE 4. Mass and lifetime projections of the B_s fit result.

$(3.4 \pm 0.5)\text{x}10^{-9}$ and $\text{BR}(\text{B}_\text{d} \to \mu^+\mu^-) = (1.00 \pm 0.14)\text{x}10^{-10}$, below CDF sensitivity. However, in several SUSY scenarios such as MSSM, RPV and mSUGRA these branch-

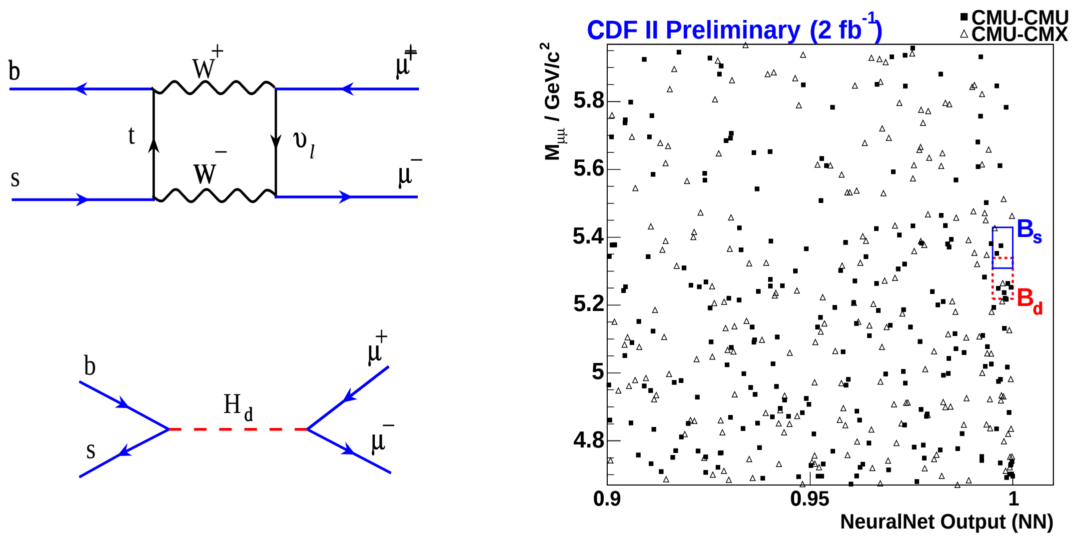

FIGURE 5. Top-Left: a SM box diagram for $B_s \to \mu\mu$ decay. Bottom-Left: SUSY decay enhanced by Higgs flavor violating diagram. Right: Dimuon invariant mass versus NN output for dimuon candidates.

ing ratios can be boosted by a factor of the order of 100 due to diagrams such as the one shown in figure 5 (bottom-left). Using a neural network (NN) to select signal and suppress backgrounds in 2 fb^{-1} of data, CDF searches for $B \to \mu^+\mu^-$ decays. Figure 5 (right) shows the invariant mass distribution vs NN output for dimuon candidates. No significant excess is found, and the following 95% confidence level (CL) limits are set on the branching ratios:

- $\mathrm{BR}(\mathrm{B_s} \to \mu^+\mu^-) < 5.8\mathrm{x}10^{-8}$ @ 95% CL
- $\mathrm{BR}(\mathrm{B_d} \to \mu^+\mu^-) < 1.8\mathrm{x}10^{-8}$ @ 95% CL

These are the best limits to date.

Charm Mixing ($D^0 - \bar{D}^0$)

The first evidence for charm mixing was presented by BELLE and BaBar in 2007. Since charm is an up-type quark, top cannot participate in the mixing loops and the resulting mixing is suppressed compared to that in the bottom and strange sectors. Using 1.5 fb^{-1} of data, CDF has found evidence of charm mixing from the study of the charm meson decays $D^{*+} \to \pi^+ D^0 \to \pi^+ K^- \pi^+$, which is a Cabibbo favored ("right sign", RS) decay, and $D^{*+} \to \pi^+ D^0 \to \pi^+ K^+ \pi^-$, which results either from D^0 mixing or from a doubly Cabibbo suppressed ("wrong sign", WS) decay. The ratio of WS to RS decays as a function of time can be expressed as $R(t) = R_d + y'\sqrt{R_d}t + (x'^2 + y'^2)t^2/4$, where x' and y' are the charm sector mixing parameters which are related to Δm and $\Delta\Gamma$ of the D^0_L and D^0_H mass eigenstates. Figure 6 shows a fit to the ratio of WS to RS charm

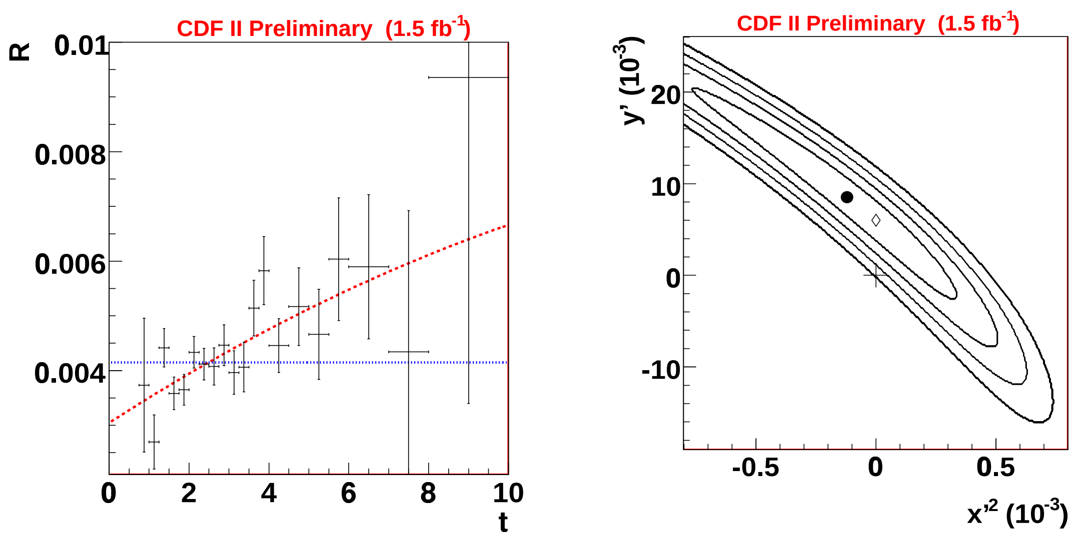

FIGURE 6. Left: Ratio of "wrong sign" to "right sign" charm meson decays as a function of proper time, and resulting fit to $R(t)$. Right: Bayesian probability contours in the x'^2-y' plane. The contours correspond to 1,2,3 and 4 standard deviations. The solid point is the result of the fit to $R(t)$, the open diamond is the most probable value for physically allowed (non-negative) values of x'^2, and the cross indicates the no-mixing point (0,0).

meson decays as a function of D^0 lifetimes, as well as the resulting Bayesian probability contours in the x'^2-y' plane. The no-mixing point ($x'^2 = y' = 0$) lies outside the contour equivalent to 3.8σ, with a probability of 0.013%. This constitutes evidence for charm mixing with a significance competitive to that of BELLE and BaBar.

At the Tevatron, W and Z bosons are predominantly produced through $q\bar{q}$ annihilation and identified mostly by their decay into electrons or muons. The study of their properties constitute an important test of the SM. The large samples of W and Z candidate events collected by CDF allow precise measurements of several electroweak observables, such as inclusive and differential cross sections, W mass, width and charge asymmetry, diboson production and gauge boson self-couplings.

W Mass and Width

The W mass and width are important parameters of the SM. Radiative corrections to M_W are dominated by Higgs and top-bottom loops, and therefore a precise determination of the top and W mass place an indirect constrain on the mass of the SM Higgs boson. A precise measurement of Γ_W provides a stringent test of SM predictions. The W mass and width are measured using 200 and 350 pb^{-1} of data, respectively. Candidate W boson events are selected by requiring an isolated, high energy electron or muon and large missing transverse energy ($\not\!\!E_T$) due to the undetected neutrino. A Monte Carlo simulation is used to predict the charged lepton p_T, the $\not\!\!E_T$ and the W transverse mass distributions as a function of M_W and Γ_W.

The W mass is extracted from template fits to the p_T of the leptons and to the transverse mass, defined as $M_W^T = \sqrt{2 p_T^\ell p_T^\nu \cos(\Delta\phi)}$, where $\Delta\phi$ is the difference in azimuthal angle between the charged lepton and the neutrino. The fits are performed in the regions around the peak of the distributions. Figure 7 shows a transverse mass

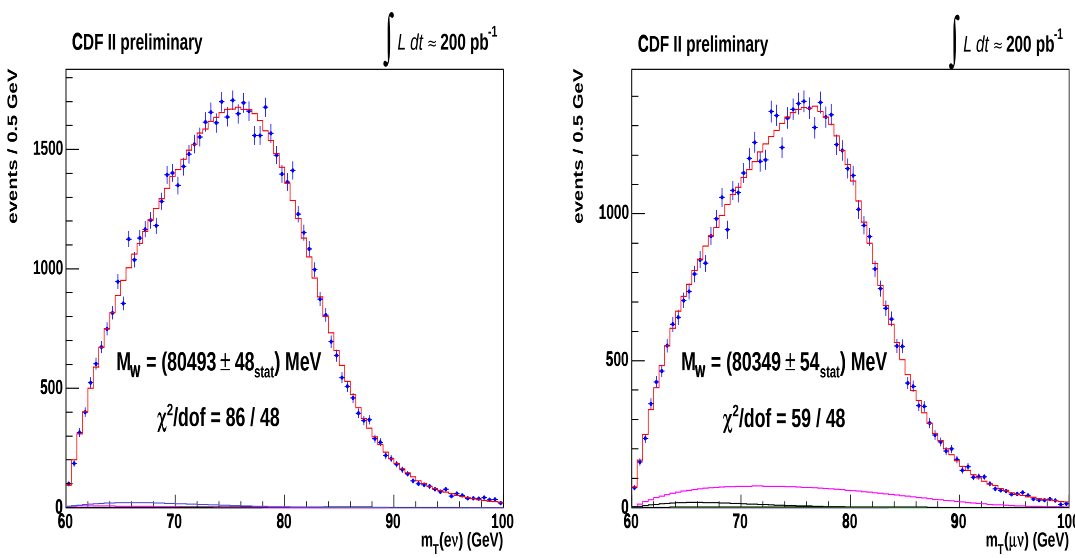

FIGURE 7. Transverse mass fits for M_W in $W \to e\nu$ (left) and $W \to \mu\nu$ (right) events.The fit is performed in the region 65-90 GeV/c^2.

fit for $W \to e\nu$ and $W \to \mu\nu$ candidate events. Combining electron and muon channels with fits to p_T^ℓ and $\not{E}_T$ yields $M_W = 80413 \pm 34(\mathrm{stat}) \pm 34(\mathrm{syst})$ MeV/c^2, the world's most precise single measurement with a total uncertainty of 48 MeV/c^2.

The W width is extracted from template fits in the high M_W^T tail region, which is most sensitive to Γ_W. Figure 8 shows a transverse mass fit for $W \to e\nu$ and $W \to \mu\nu$ candidate

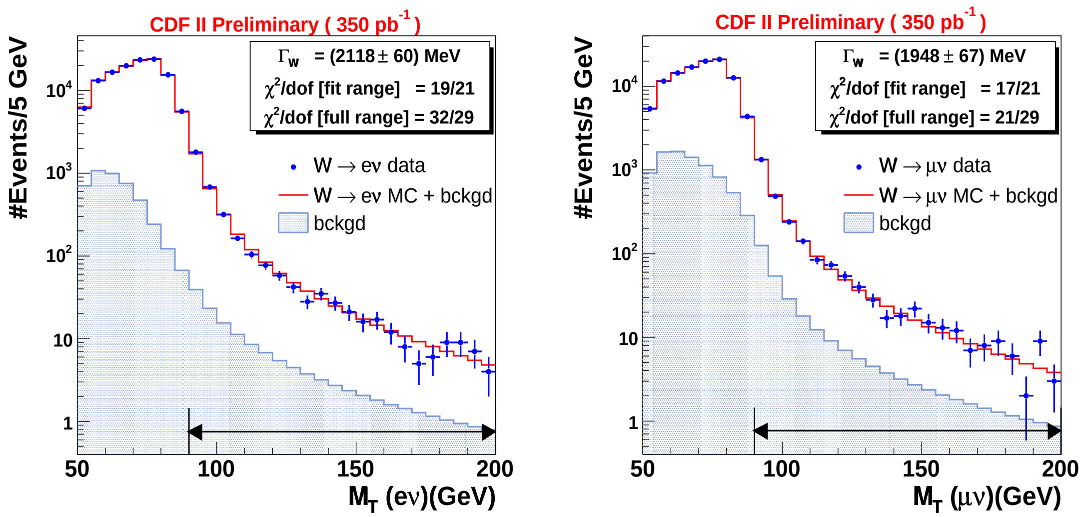

FIGURE 8. Transverse mass fits for Γ_W in $W \to e\nu$ (left) and $W \to \mu\nu$ (right) events. The fit is performed in the region 90-200 GeV/c^2.

events. Combining electron and muon channels yields $\Gamma_W = 2032 \pm 71$ MeV/c^2, the world's most precise single measurement, in good agreement with SM predictions.

WZ and ZZ Production

While W and Z vector bosons are readily produced at the Tevatron, pair production of vector bosons is far more rare. These processes probe gauge boson self interactions, an important consequence of the $SU(2)_L \otimes U(1)_Y$ structure of the SM. Cross sections which deviate from SM predictions would be indicative of physics beyond the SM. CDF measures the WZ and ZZ cross sections in events with multiple leptons and/or large $\not{E}_T$ in the final state, yielding a low number of events but very clean signatures. These analysis benefit greatly from an improved lepton acceptance which results from exploiting all available detector information when defining leptons.

The WZ cross section is measured in a 1.9 fb^{-1} data sample using events with three charged leptons and large $\not{E}_T$ in the final state. The cross section times branching ratio is low, but the signal is very clean. A total of 25 events pass the WZ selection requirements, with a SM prediction of 22 ± 3 events. Figure 9 (left) shows the $\not{E}_T$ distribution for WZ candidate events compared with the SM expectations. The measured cross section is $\sigma(WZ) = 4.3^{+1.4}_{-1.1}$ pb, where the uncertainty is largely dominated by the statistical uncertainty. This is in good agreement with the SM NLO prediction of 3.7 ± 0.3 pb.

The ZZ cross section is measured in a 1.1 fb^{-1} data sample. The selection of four isolated, energetic charged leptons yields only one event over an expected SM total

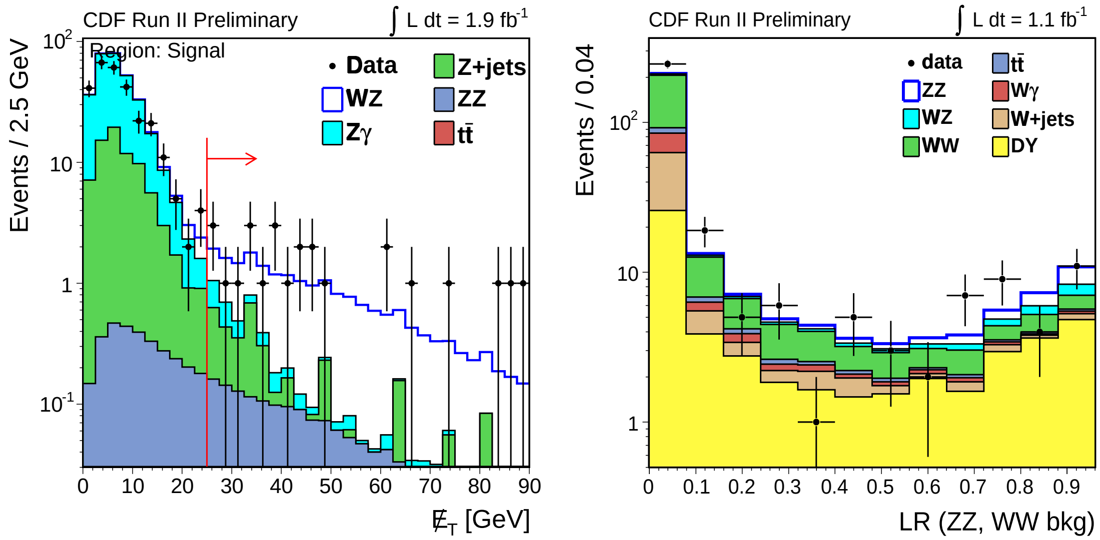

FIGURE 9. $\not{E}_T$ distribution for $WZ \to \ell\ell\ell\nu$ candidates compared to SM expectations (left), and distribution of the likelihood ratio (LR) for $ZZ \to \ell\ell\nu\nu$ candidates (right).

of 2.5 events. The cross section is measured in the $ZZ \to \ell\ell\nu\nu$ channel by selecting events with large $\not{E}_T$ and two oppositely charged, same flavor leptons with invariant mass close to the Z mass. In order to separate ZZ from the WW background, an event-by-event probability is calculated based on all the available kinematic information. Figure 9 (right) shows the resulting likelihood ratio discriminant (LR), which is fit to extract the signal yield. Combining with the four charged lepton channel, the measured cross section is $\sigma(ZZ) = 0.75^{+0.71}_{-0.54}$ pb, the smallest cross section ever measured at a hadron collider, with a signal significance of 3σ. This is consistent with the SM NLO prediction of 1.4 ± 0.1 pb.

TOP PHYSICS

The top quark, discovered in 1995 by the CDF and D0 collaborations, is the heaviest known fundamental particle. Its Yukawa coupling to the SM Higgs is roughly one, and therefore top might play a special role in electroweak symmetry breaking. Because of its large mass, radiative corrections to other SM observables are dominated by loops involving top, and depend strongly on the top mass. A precise determination of M_t and M_W helps constrain the mass of the SM Higgs boson.

At the Tevatron, top is mainly produced in $t\bar{t}$ pairs via the strong interaction in quark-antiquark annihilation and gluon-gluon fusion. Single top production has a smaller cross section and involves electroweak production of a top quark via the Wtb vertex by a t or s channel exchange of a virtual W boson. Once produced, it decays virtually 100% of the time into a W and a b, $t \to Wb$. The top lifetime is so short that it decays before it has time to hadronize. The final state therefore depends on the disintegration mode of the W bosons and has jets from the hadronization of b quarks.

$t\bar{t}$ Cross Section

Measuring the $t\bar{t}$ production cross section in different channels is an important test of pQCD predictions. In addition, the cross section analysis establish a baseline for top quark samples which are used to study other top properties such as the mass, and to estimate top related backgrounds, which are important in many searches for physics beyond the SM. Since top production has a very small cross section and the backgrounds are typically large, these analysis need an event selection to obtain a data sample with good S/B, and a precise determination of the dominant backgrounds and of the overall signal acceptance. Figure 10 (left) shows the signal and background

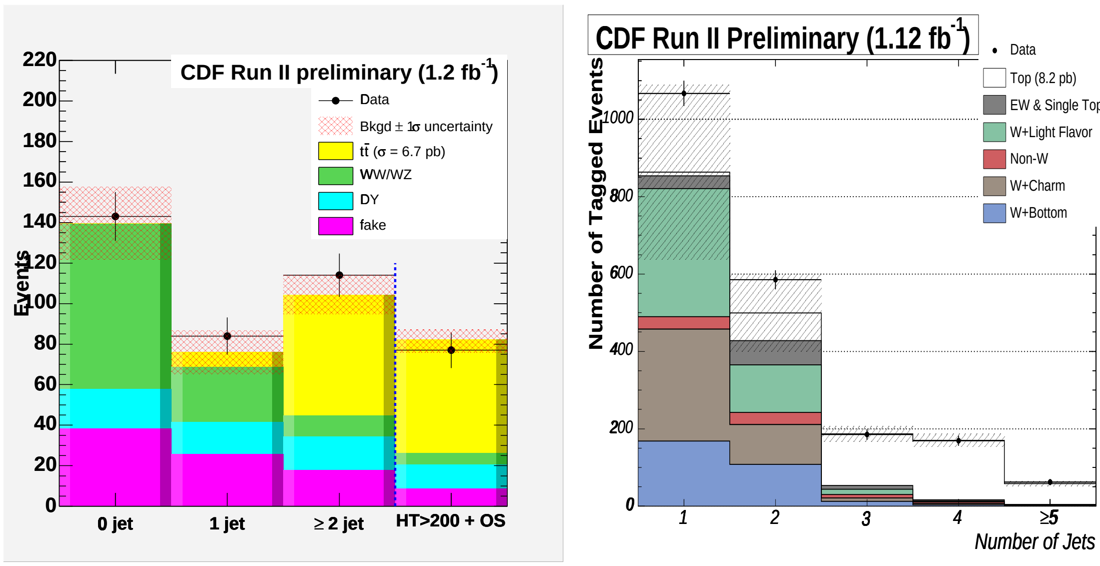

FIGURE 10. Summary of backgrounds and signal as a function of jet multiplicity for $t\bar{t}$ cross section measurements in the dilepton channel (left) and in the lepton+jets channel with b tagging (right). The low jet multiplicity bins are used as control regions and the cross section is measured in the large jet multiplicity bins, with large $t\bar{t}$ acceptance.

contributions as a function of jet multiplicity for the "dilepton" $t\bar{t}$ sample, where both W bosons decay into electron or muon. The zero and one jet bins, where one expects little top contribution, are used as a control region, and the cross section is measured in the bin with ≥ 2 jets, where most of the top signal is expected. The measured cross section is $\sigma_{t\bar{t}} = 6.16 \pm 1.05(\text{stat}) \pm 0.72(\text{syst}) \pm 0.37(\text{lumi})$ pb. Figure 10 (right) shows the signal and background contributions for the "lepton+jet" $t\bar{t}$ sample, where one W decays into electron or muon and the other to quarks (resulting in more jests in the final state). In order to enhance the top to background ratio, events are required to have at least one b-tagged jet. The one and two jet bins are used as control regions and the cross section is measured in the three, four and ≥ 5 jet bins. The measured cross section is $\sigma_{t\bar{t}} = 8.2 \pm 0.5(\text{stat}) \pm 0.8(\text{syst}) \pm 0.5(\text{lumi})$ pb.

CDF measures the $t\bar{t}$ cross sections in many different channels and finds all measurements to be consistent with each other and with theoretical predictions, as shown in figure 11.

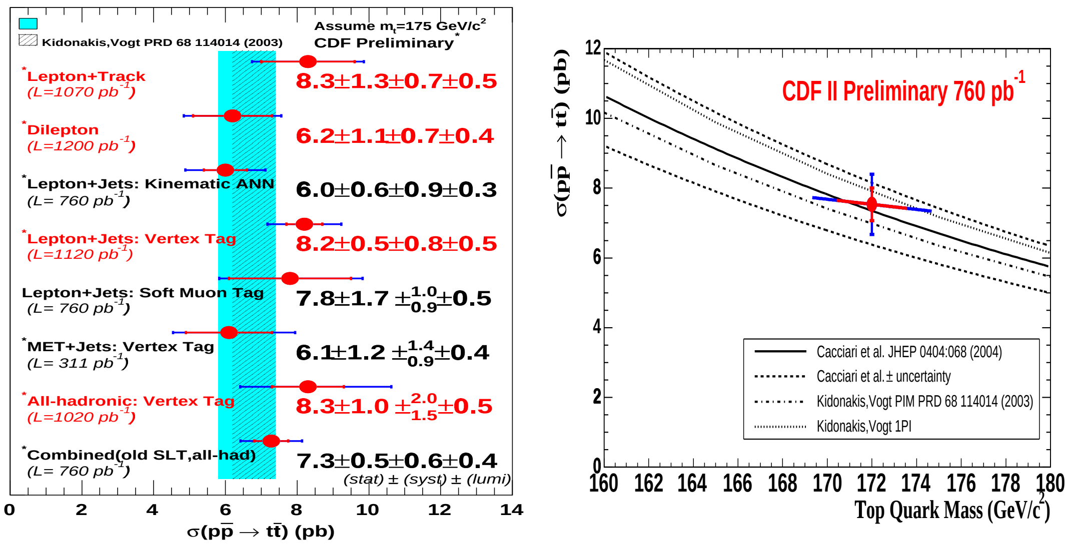

FIGURE 11. Summary of CDF $t\bar{t}$ cross section measurements (left), where a top mass of 175 GeV is assumed for acceptance calculations, and comparison of $t\bar{t}$ cross section and top mass measurements with theoretical predictions (right).

Single Top

Single top production is interesting because it probes the Wtb electroweak vertex, allowing a direct measurement of the V_{tb} CKM matrix element. The NLO production cross sections predicted at the Tevatron are $\sigma_s = 0.88 \pm 0.11$ pb for s-channel production and $\sigma_t = 1.98 \pm 0.25$ pb for the t-channel [4]. The tiny cross sections, combined with very large backgrounds, make it impossible to extract a single top signal using conventional counting experiments. Instead, multivariate techniques such as matrix element discriminants or multivariate likelihoods are required. Using these sophisticated analysis techniques, combined with more integrated luminosity, CDF has found evidence for single top production and measured its cross section. Figure 12 (left) shows the multivariate likelihood distribution for data and the expected contributions from single top and backgrounds. The observed signal significance is 2.7σ and the overall single top cross section (both s and t channels) is measured to be $sigma_{s+t} = 2.7 \pm 1.2$ pb. Figure 12 (right) shows the matrix element event probability discriminant for data and the expected contributions from single top and backgrounds. The observed signal significance is 3.1σ and the measured cross section is $sigma_{s+t} = 3.0 \pm 1.2$ pb. Assuming a SM ($V-A$, CP conserving) Wtb vertex, these measurements can be translated into a direct measurement of V_{tb}, yielding $V_{tb} = 1.02 \pm 0.18(\text{experiment}) \pm 0.07(\text{theory})$.

Top Mass

The top mass is a fundamental parameter of the SM. As stated earlier, a precise determination of M_t helps constrain the SM Higgs mass and reduces the uncertainties

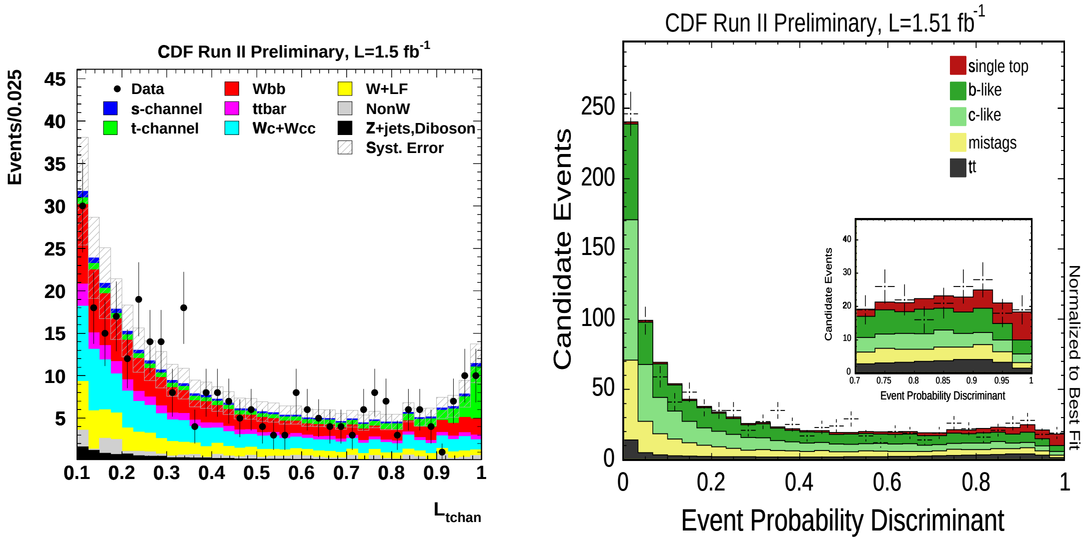

FIGURE 12. Multivariate likelihood distribution (left) and matrix element event probability discriminant (right) for data and for the expected single top and background contributions.

of dominant radiative corrections to other SM observables. The reconstruction of the top mass presents several experimental challenges. Quarks hadronize to form jets whose energy must be corrected back to the parton level, making it crucial to have a precise jet energy scale (JES). The assignment of the observed final state jets to the partons from the leading order $t\bar{t}$ production process usually has several possible permutations, a problem which becomes even worse with the presence of gluons from initial and final state radiation. Neutrinos from leptonic W decays escape detection, and their undetermined longitudinal momentum gives rise to non-unique "neutrino solutions". Finally, top samples have non-negligible backgrounds which must be accounted for in the mass determination.

CDF has performed the world's most precise single top mass measurement based on a 1.7 fb^{-1} data sample using events with one lepton, large $\not{E}_T$, and exactly four energetic jets, at least one of which must be b tagged. The analysis uses a 10 variable neural network discriminant to separate signal from background, as shown in figure 13 (top left). The jet energy scale is measured "in-situ" from hadronic W decays, and a signal likelihood is calculated event by event using a matrix element integration method. The combined overall signal probability is a 2-D likelihood as a function of M_t and JES, shown in figure 13 (right). Figure 13 (bottom left) also shows the most likely top mass value for each of the 293 $t\bar{t}$ candidate events. The measured top mass is $M_t = 172.7 \pm 1.3(\text{stat}) \pm 1.2(\text{JES}) \pm 1.2(\text{syst}) = 172.7 \pm 2.1$ GeV/c^2.

HIGGS SEARCHES

One of the outstanding questions in particle physics is the dynamics of electroweak symmetry breaking and the origin of particle masses. In the SM, electroweak symmetry

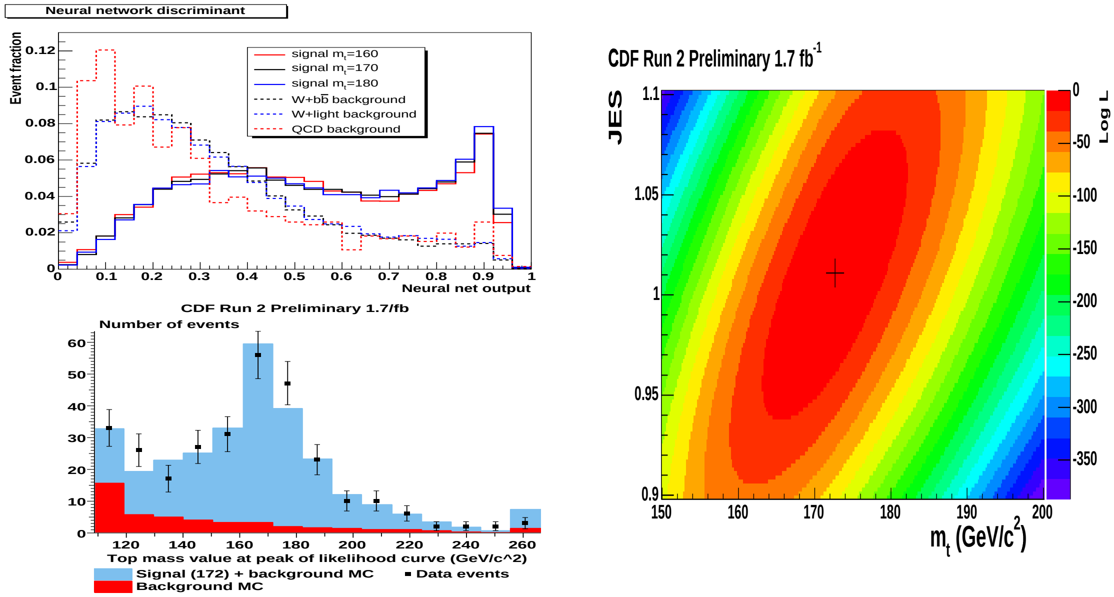

FIGURE 13. Neural network output for $t\bar{t}$ signal at different top masses and for background (top left); value of the most likely top mass for each $t\bar{t}$ candidate event (bottom left); combined 2-D likelihood as a function of M_t and JES (right).

is spontaneously broken through the Higgs mechanism by introducing a doublet of self-interacting complex scalar fields with non-zero vacuum expectation values. The physical manifestation of this scenario is the existence of a massive scalar Higgs boson. Assuming the SM to be correct, a $\Delta\chi^2$ curve can be derived from precision electroweak measurements as a function of the SM Higgs mass, M_H. Recent improvements in the combined Tevatron top mass (as of March of 2007) $M_t = 170.9 \pm 1.8$ GeV/c^2 and the combined LEP2+Tevatron W mass $M_W = 80.398 \pm 0.025$ GeV/c^2, push the most likely value of M_H down into the region excluded by LEP direct searches, as shown in figure 14. The preferred value for M_H is 76^{+33}_{-24} GeV/c^2, and at 95% CL $114 < M_H < 182$ GeV/c^2. If indeed the Higgs exists and lies in this mass range, it is within reach of the Tevatron if enough luminosity is collected. Its search is so important that it has become the top priority of the CDF collaboration.

At the Tevatron, the Higgs is mainly produced via gluon-gluon fusion (through a fermion loop). Associated production with a W or Z boson (through a virtual W or Z) has a smaller cross section, but has the advantage of an isolated lepton in the final state which helps reduce the backgrounds. The way the Higgs decays depends on its mass. The dominant decay mode for masses up to about 135 GeV/c^2 is to $b\bar{b}$. For larger masses, the dominant decay is to WW. CDF has performed several searches for SM Higgs in different channels and optimized for different Higgs masses.

For $M_H > 130$ GeV/c^2, the most sensitive channel is $gg \to H \to WW^* \to \ell\nu\ell\nu$. A matrix element method is used to calculate an event by event probability using full kinematic information, and a likelihood ratio (LR) discriminant is constructed to separate signal from background. Figure 15 (left) shows the LR distribution for data and for different sources of background, as well as the expected distribution for a Higgs

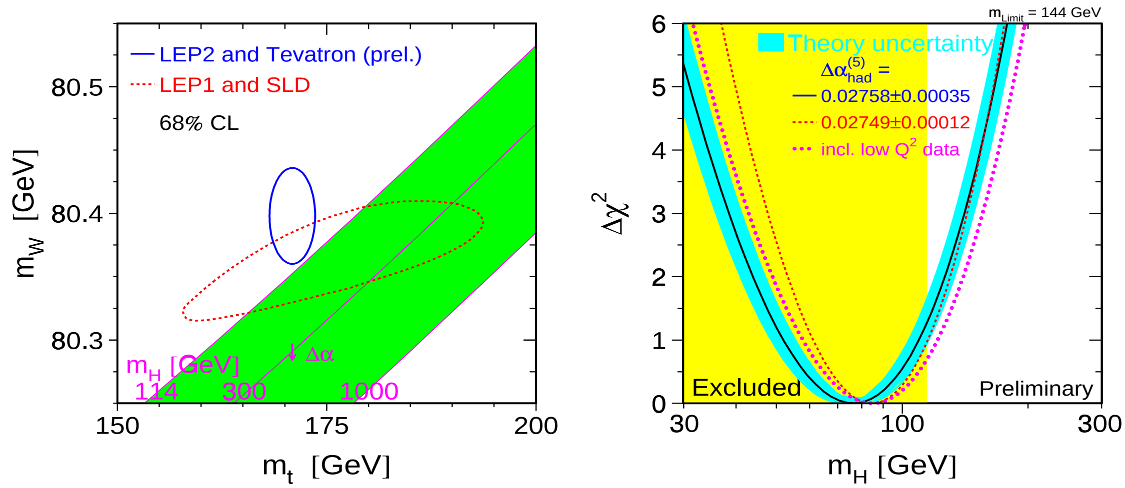

FIGURE 14. Left: Combined W and top mass values, and 1σ contour. The band shows the most likely Higgs mass as a function of M_W and M_t. Right: $\Delta\chi^2$ from precise electroweak data as a function of M_H.

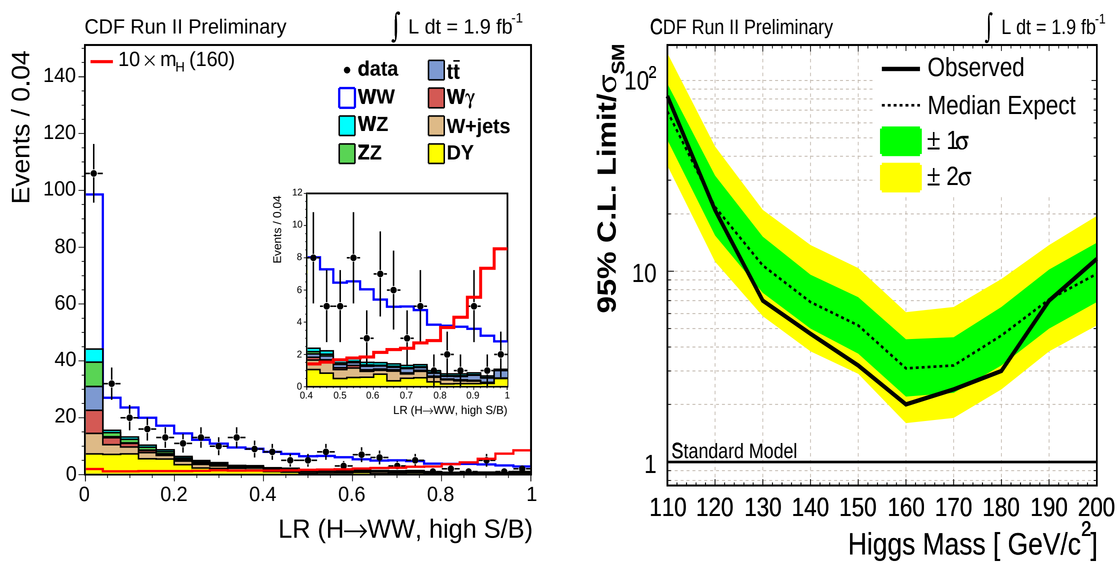

FIGURE 15. Left: Likelihood ratio discriminant distribution for data, backgrounds, and Higgs signal (blown up by a factor of 10) at $M_H = 160$ GeV/c^2. Right: 95% CL upper limit on the cross section (divided by SM cross section) as a function of M_H.

signal with $M_H = 160$ GeV/c^2 (scaled up by a factor of 10 to make it visible). This figure shows how hard it is to separate the tiny Higgs signal from the large backgrounds, in this case the WW background in particular, even using sophisticated analysis techniques. In the absence of an excess of events over SM predictions, 95% CL upper limits on the cross section are derived as a function of M_H, as shown in figure 15 (right). For a Higgs mass of 160 GeV/c^2, the observed 95% CL upper limit is 0.8 pb, equivalent to two times the SM prediction.

CDF has combined all SM Higgs searches and sets a 95% CL upper limit on the production cross section as a function of M_H, shown in figure 16 (left). Perhaps the

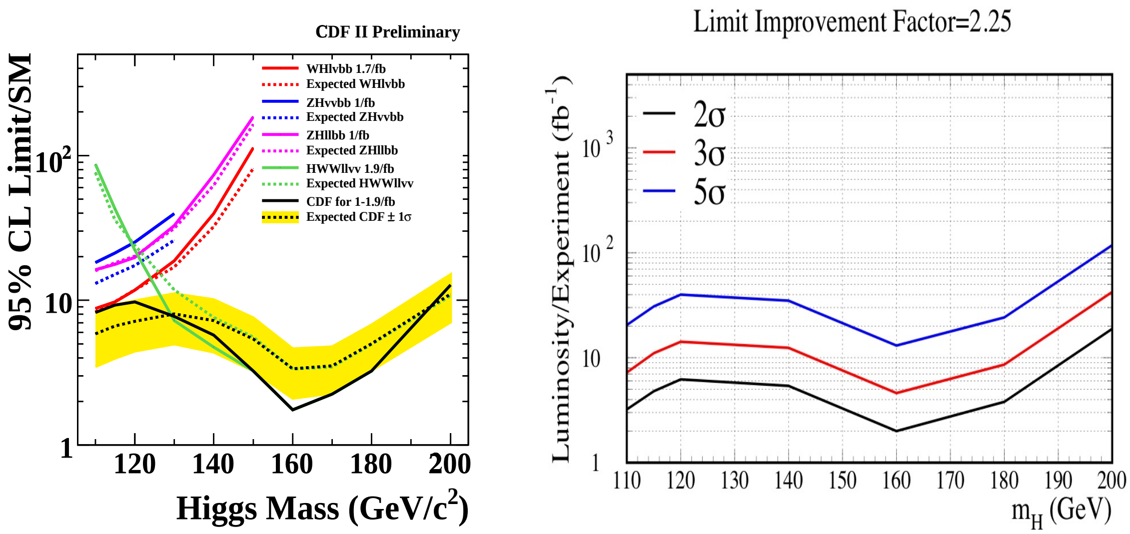

FIGURE 16. Left: CDF combined 95% CL upper limit on the SM Higgs cross section (divided by SM cross section) as a function of M_H. Right: expected Tevatron sensitivity as a function of Higgs mass and integrated luminosity (per experiment). Sensitivity curves assume an improvement of 2.25 which has been demonstrated to be achievable.

most important statements that can be made today about searches for SM Higgs involve the expected Tevatron reach. Figure 16 (right) shows the expected sensitivity as a function of integrated luminosity (per experiment) and as a function of M_H. It should be noted that the sensitivity curves shown assume an improvement of 2.25 with respect to the current sensitivities. This improvement is achievable: it has been proved in other analysis and arises from using techniques which have not yet been fully implemented in Higgs searches, such as neural network or matrix element discriminants, extended lepton acceptance, improved b tagging and inclusion of additional triggers. With an integrated luminosity of 7 fb^{-1} the Tevatron expects to exclude all masses below 188 GeV/c^2 at 2σ and to have 3σ sensitivity for evidence in the mass range 150 – 170 GeV/c^2.

SUSY Higgs Searches

Theoretical difficulties arise in the SM related to divergent radiative corrections to the Higgs mass. In order to keep the Higgs mass stable between the electroweak and the Plank scale, large quantum corrections must be very finely tuned or some new physics must intervene. The challenge of preserving the widely separated electroweak and Plank scales in the presence of quantum corrections is known as the hierarchy problem. Supersymmetric models offer a natural solution to this problem. The minimal supersymmetric extension of the standard model (MSSM) requires two Higgs doublets resulting in a Higgs sector with two charged and three neutral bosons. One of the neutral bosons is *CP*-odd (A), and the other two are *CP*-even (h, H). The symbol ϕ is used to denote any of h, H or A. The leading decay modes for the neutral MSSM Higgs are $\phi \to b\bar{b}$ (90%) and $\phi \to \tau\bar{\tau}$ (10%).

CDF has performed several searches for charged and neutral SUSY Higgs. For large values of $\tan\beta$, the ratio of Higgs coupling to down-type versus up-type quarks, the production of light neutral Higgs in association with b-quarks can be significantly enhanced. We search for the process $\phi + b \to bb + b$ by selecting events with three b-tagged jets with $E_T > 20$ GeV. The dominant backgrounds are *QCD* heavy flavor production and light jets misidentified as b jets. We study the invariant mass of the

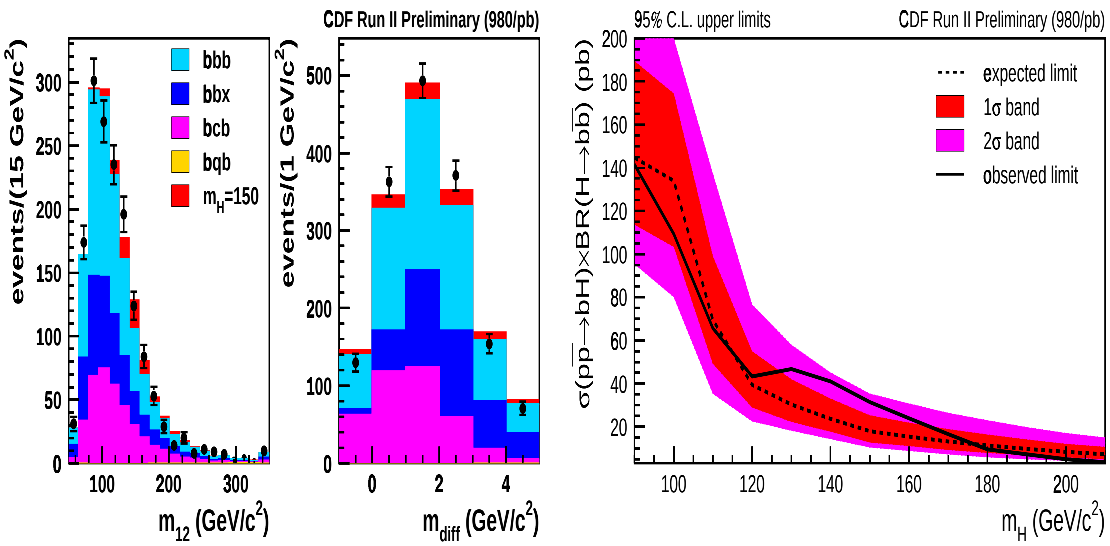

FIGURE 17. Left: Fit of the triple-tagged data sample to *QCD* background templates and signal of Higgs with mass 150 GeV/c^2. Right: Median, 1σ and 2σ expected limits and observed 95% CL upper limits on cross section times BR as a function of Higgs mass.

two leading jets, M_{12}, and $M_{\text{diff}} \equiv M^{\text{jet1}}_{\text{vertex}} + M^{\text{jet2}}_{\text{vertex}} - M^{\text{jet3}}_{\text{vertex}}$, related the mass of the tracks forming the displaced vertexes. The distributions observed in the triple-tagged data sample are fit to background templates and to signal shapes for different values of the Higgs mass, as shown in figure 17. No excess of events is observed over the SM expectation, and therefore 95% CL upper limits are derived on the production cross-section times branching ratio, shown in figure 17 (right). Expected limits are derived from pseudo-experiments where the fits are performed to background-only distributions.

These limits can be trivially converted into limits on $\tan\beta$ versus pseudoscalar mass m_A in MSSM models by dividing by the SM cross-section times branching ratio and taking the square root. The result is shown in figure 18 (left). These limits do not include potentially large loop corrections and Higgs width effects, which make the limits worsen quickly at high $\tan\beta$. Limits were also generated for the m_h^{max} scenario [5], which maximizes the mass of the lighter scalar Higgs h and allows conservative exclusion bounds, with $\mu = -200$ GeV, shown in figure 18 (right). Here the limits remain tight due to large and negative values of loop corrections.

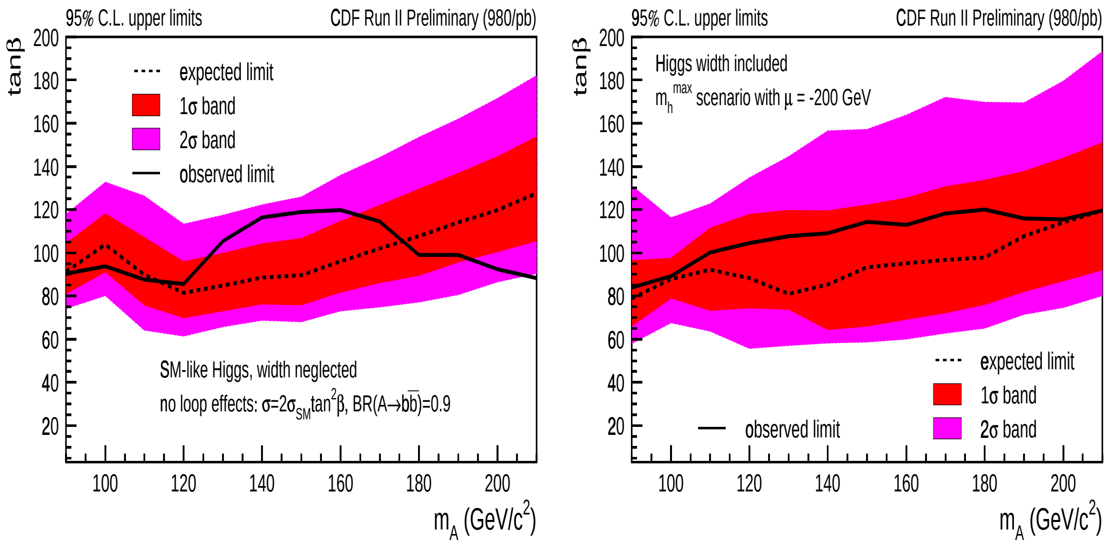

FIGURE 18. Left: $\tan\beta$ limits as a function of m_A not including loop corrections or Higgs width effects. Right: $\tan\beta$ limits for the $m_h^{\max}$ scenario with $\mu = -200$ GeV, including Higgs width effects, as a function of m_A.

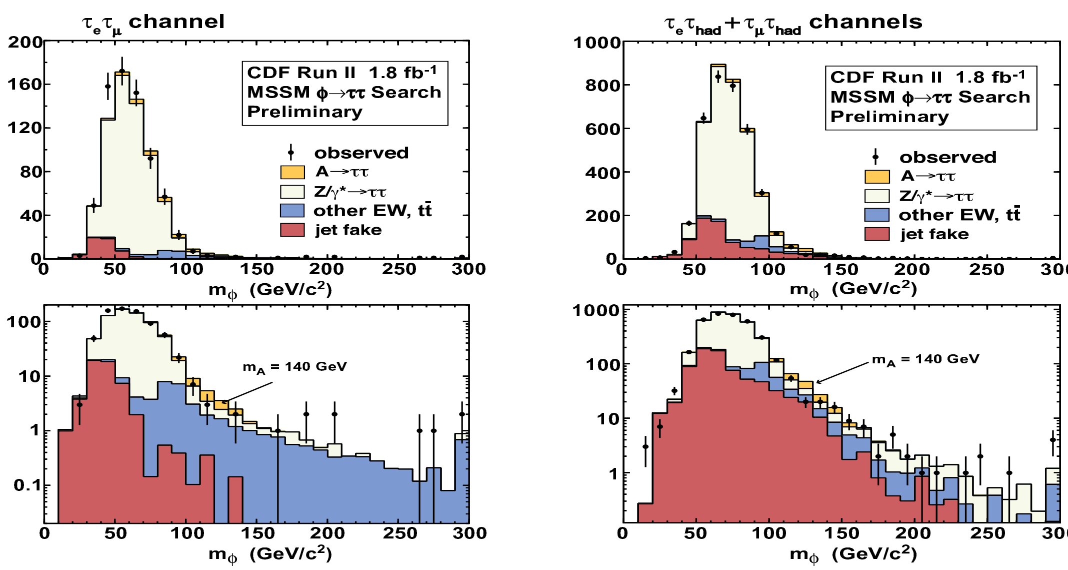

FIGURE 19. Fit of the partially reconstructed di-τ mass to background and signal with Higgs mass of 140 GeV for the $\tau_e\tau_\mu$ (left) and $\tau_e\tau_{had} + \tau_\mu\tau_{had}$ (right) final states.

Despite the smaller BR into taus, Higgs searches in the di-τ channel do not suffer from such large QCD backgrounds. A search was performed for $\phi \to \tau\bar{\tau}$ by selecting events with tau pairs in three final states: $\tau_e\tau_{had}$, $\tau_\mu\tau_{had}$ and $\tau_e\tau_\mu$, where τ_e, τ_μ and τ_{had} denote the decay modes $\tau \to e\nu_e\nu_\tau$, $\tau \to \mu\nu_\mu\nu_\tau$ and $\tau \to$ hadrons ν_τ, respectively. The dominant background is $Z/\gamma^* \to \tau\tau$. The partially reconstructed mass of the di-τ system is defined as the invariant mass of the visible tau decay products and the $\not{E}_T$,

$m_{\text{vis}} = \sqrt{p_{\tau_1}^{\text{vis},2} + p_{\tau_2}^{\text{vis},2} + \not{E}_T^2}$. This distribution is fit to a combination of background and signal generated at different Higgs masses, as shown in figure 19. No excess of events over the SM prediction is observed, and upper limits at 95% CL are set on the cross section times branching ratios. Figure 20 shows the upper limits and their MSSM interpretation as exclusion regions in the $\tan\beta$-m_A plane for the $m_h^{\max}$ MSSM scenarios with positive and negative sign of μ.

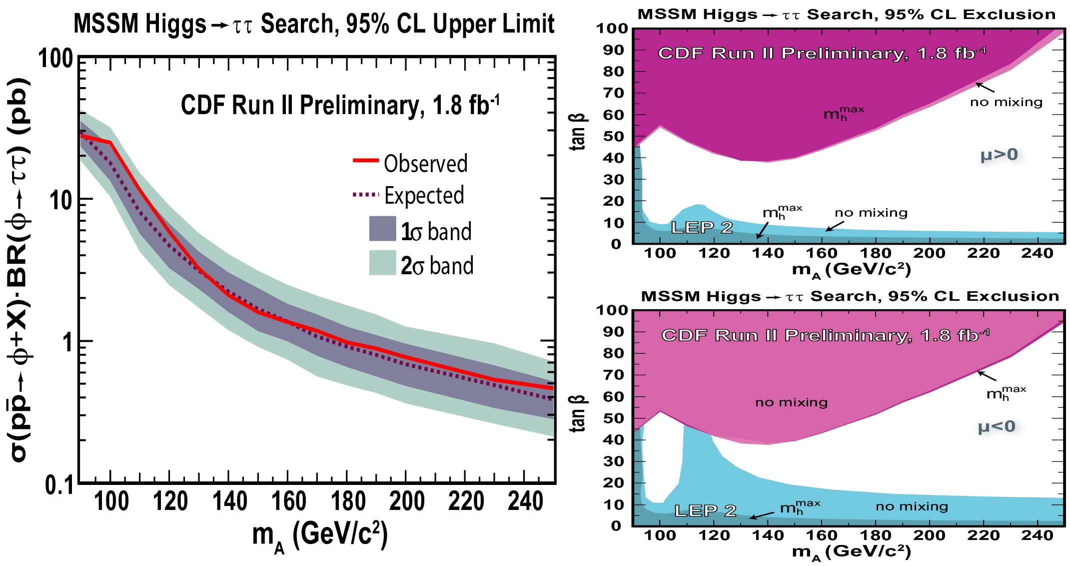

FIGURE 20. Left: 95% CL upper limit on cross section times BR as a function of m_A. Right: $\tan\beta$ limits for the $m_h^{\max}$ scenario with positive (top) and negative (bottom) sign of μ as a function of m_A.

OTHER BEYOND SM SEARCHES

Apart from SUSY Higgs, CDF searches for sparticles and gauginos, also predicted by SUSY models, and for manifestations of physics beyond the standard model (BSM) in several alternative theoretical scenarios, including additional heavy gauge bosons, gravitons, extra dimensions, technicolor, leptoquarks, and deviations from SM predictions in several signatures. A few of the most recent BSM searches are described below.

Search for Squarks/Gluinos

In the minimal supergravity scenario (mSUGRA) with R-parity conservation, all sparticles except the neutralino are unstable and decay into their SM counterparts. This cascade decays result in a final state with several jets from the squarks and gluinos, and large $\not{E}_T$ from the undetected neutralinos. Events are selected with 2,3 or 4 high energy jets plus large $\not{E}_T$. Events with identified leptons are rejected, and cuts on azimuthal separation between jets and $\not{E}_T$ are used to reduce the QCD backgrounds. The resulting $\not{E}_T$ distribution is fit to a combination of backgrounds and signal generated at different gluino/squark masses. The observed distributions agree with the SM predictions, and upper limits are set on the cross section as a function of squark and gluino masses. From these limits, lower limits are obtained for the squark and gluino masses. These limits are combined to obtain a 95% CL exclusion region in the $M_{\tilde{g}}$-$M_{\tilde{q}}$ plane, shown in figure 21 (left). A scan is performed in the M_0-$M_{1/2}$ plane (the common scalar and fermion masses

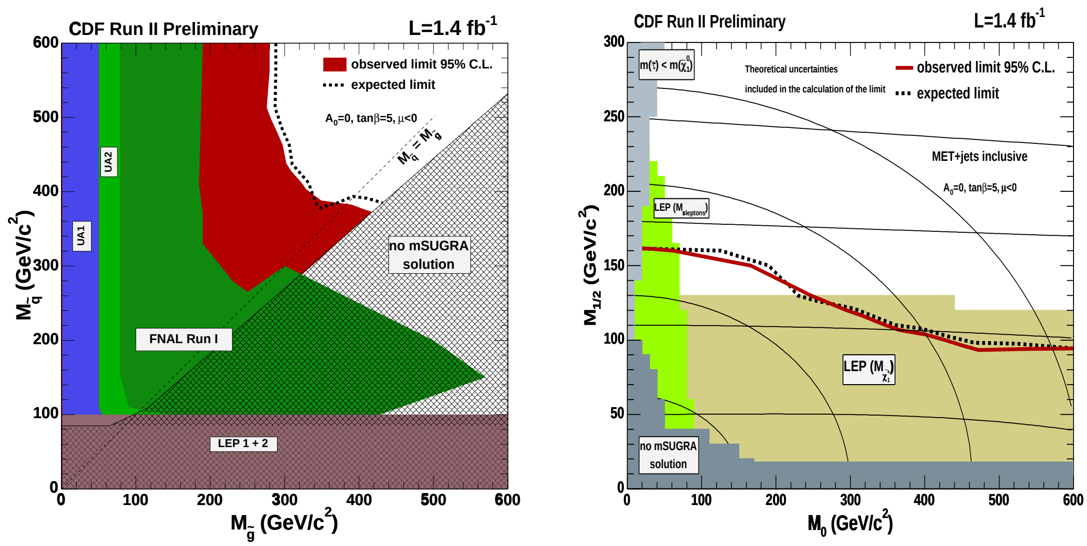

FIGURE 21. Left: 95% CL exclusion region in the $M_{\tilde{g}}$-$M_{\tilde{q}}$ plane. Right: 95% CL exclusion region in the M_0-$M_{1/2}$ plane for the mSUGRA scenario with $A_0 = 0$, negative μ and $\tan\beta = 5$.

at the GUT scale) for the mSUGRA scenario with $A_0 = 0$, negative μ and $\tan\beta = 5$, and the resulting exclusion region is shown in figure 21 (right). At low values of M_0 and $M_{1/2}$ these limits extend the region excluded by LEP.

Search for Charginos/Neutralinos

Strong sparticle production at the Tevatron is suppressed owing to the large squark and gluino masses inferred from the limits shown above. The associated production of $\tilde{\chi}_1^{\pm}\tilde{\chi}_2^0$ is therefore likely to be the dominant SUSY production mechanism. CDF has performed a search for the process $p\bar{p} \to \tilde{\chi}_1^{\pm}\tilde{\chi}_2^0$ followed by $\tilde{\chi}_2^0 \to \ell\ell\tilde{\chi}_1^0$ and $\tilde{\chi}_1^{\pm} \to \ell\nu\tilde{\chi}_1^0$, which results in a striking trilepton plus $\not{E}_T$ signature. In order to gain acceptance for events with a soft third lepton, events with only two energetic, like sign (LS) leptons are also considered. The SM backgrounds are small, dominated by Drell-Yan, dibosons, and $W/Z+\gamma$. No significant excess of events is observed for the different trilepton and LS topologies compared to SM predictions. As no evidence of SUSY is observed, results from the different topologies are combined to obtain limits on the cross section times BR for some points in parameter space of the model. Figure 22 shows 95% CL upper limits for the $\tilde{\chi}_1^{\pm}\tilde{\chi}_2^0$ production cross section times BR as a function of the chargino mass for two scenarios: mSUGRA with $\tan\beta = 3$, $A_0 = 0$, $\mu > 0$ and $M_0 = 60$ and an MSSM scenario which keeps the same relations as mSUGRA but with no sletpon mixing, which enhances the BR of charginos and neutralinos to electrons and muons. In the mSUGRA scenario the expected limit is sensitive to chargino masses of about 125 GeV/c^2. For the

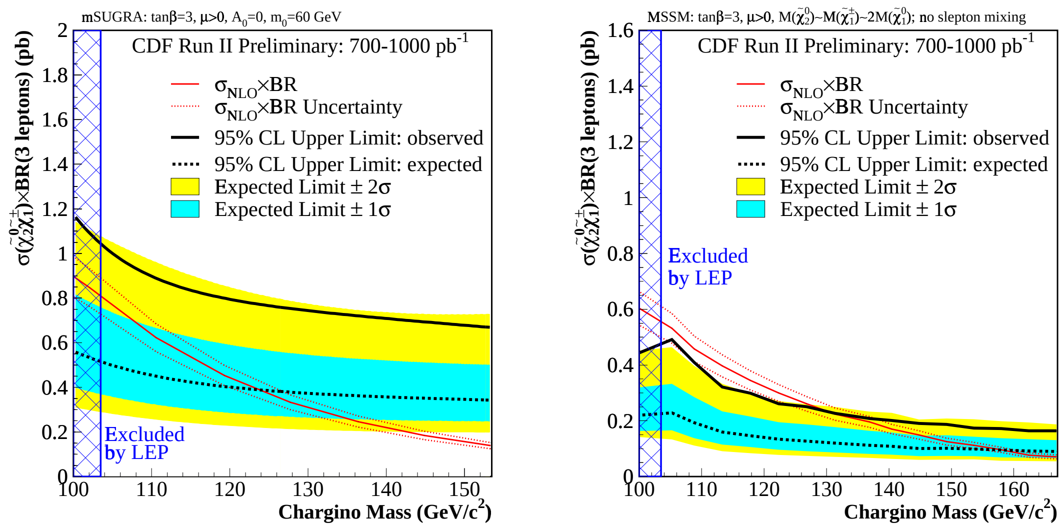

FIGURE 22. 95% CL upper limits on $\tilde{\chi}_1^{\pm}\tilde{\chi}_2^0$ production cross section times branching ratio as a function of chargino mass for the mSUGRA (left) and MSSM (right) scenarios described in the text.

MSSM scenario considered, chargino masses below 129 GeV/c^2 are excluded at 95% CL.

Search for Large Extra Dimensions

Compactified Large Extra Dimensions (LED) have been proposed [6] as an alternative solution to the hierarchy problem between the weak and gravitational scales. In these models, only gravitons (G) can propagate in the n extra dimensions of the $4+n$ dimensional bulk of spacetime. The resulting effective (or reduced) Plank scale, M_D, is related to the Plank scale and to the extent R of the extra dimensions through $M_{\text{Plank}}^2 \sim R^n M_D^{2+n}$. The large value of the Plank scale is therefore due to the large extent of the extra dimensions. The predicted gravitons are produced directly in processes such as $q\bar{q} \rightarrow gG$, $qg \rightarrow qG$ and $gg \rightarrow gG$, resulting in a highly energetic mono-jet signature accompanied by large $\not{E}_T$ from the undetected graviton. CDF searches for these processes by selecting events with one highly energetic jet ($E_T > 150$ GeV) and large $\not{E}_T$ (> 120 GeV). A second jet with $E_T < 60$ GeV is allowed in order to gain some acceptance. Figure 23 (left) shows the $\not{E}_T$ distribution of the selected events superimposed with the SM predictions and with the expected distribution for LED signal with $n = 2$ and $M_D = 1$ TeV. No excess of events is found over SM predictions, and 95% CL lower limits are derived on the reduced Plank scale as a function of the number of extra dimensions, shown in figure 23 (right). For $n > 3$, these are the best available limits on M_D.

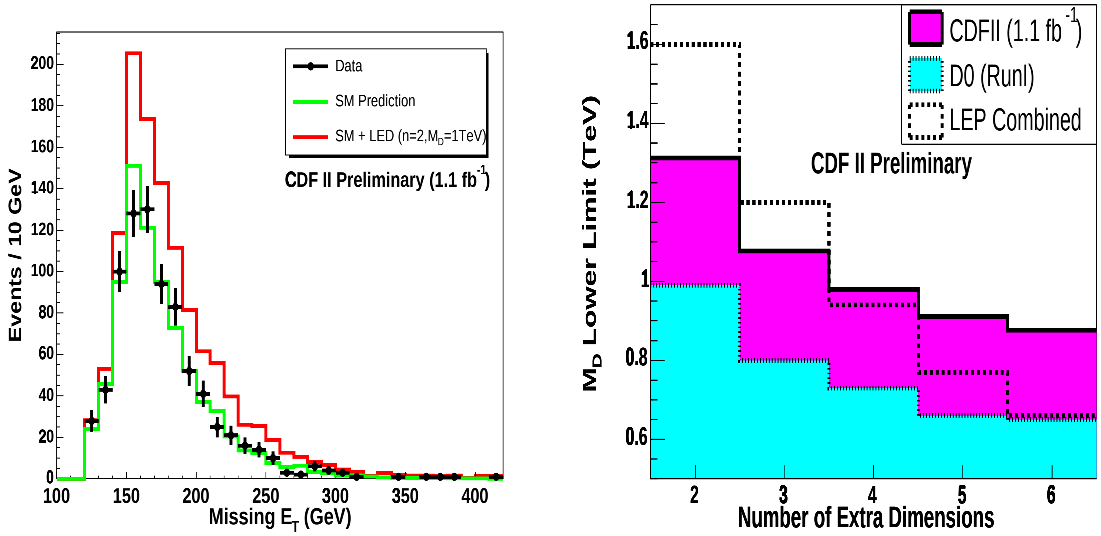

FIGURE 23. Left: the $\not\!\!E_T$ distribution observed in data and the predicted distributions for SM-only and SM+LED signal with $n = 2$ and $M_D = 1$ TeV. Right: 95% CL lower limits on M_D as a function of the number of extra dimensions.

Search for High Mass Resonances

Several extensions of the SM predict the existence of new particles decaying into lepton or photon pairs, such as Z' predicted in GUT theories [7] or Randall-Sundrum (RS) gravitons. The Randal-Sundrum model [8] is a theory of extra dimensions in which a warp factor determines the curvature k of the extra dimensions and therefore the mass of the Kaluza-Klein graviton resonances. Searches for dilepton or diphoton resonances are broad, inclusive and sensitive. Discovery of a sharp mass peak over background would be compelling evidence of a new particle. CDF has searched for resonances in dielectron, dimuon, dijet and diphoton final states. Figure 24 shows the invariant mass distribution for dielectron (left) and diphoton (right) final states. As no significant excess is found over SM predictions, 95% CL upper limits are derived on the cross section times BR as a function of the new particle mass. Figure 25 shows the limits for the dielectron final state as a function of $M_{Z'}$ (left), and the limits for the dielectron, diphoton, and combined $ee+\gamma\gamma$ final states as a function of M_G (right). Lower limits can be inferred for the new particle masses when the cross section limits are compared to different theoretical scenarios. For example, for a Z' with SM couplings, the dielectron limit implies $M_{Z'} > 923$ GeV/c^2 at 95% CL, and the combined limit implies that $M_G > 889$ GeV/c^2 for a RS model with $k/M_{\rm Plank} = 0.1$. Figure 26 shows the 95% CL excluded region on the $k/M_{\rm Plank}$-M_G plane, the most exclusive limit to date.

CONCLUSIONS AND OUTLOOK

The CDF collaboration has been very active in all aspects of its broad physics program, with constantly maturing and improving analysis covering a wide range of topics.

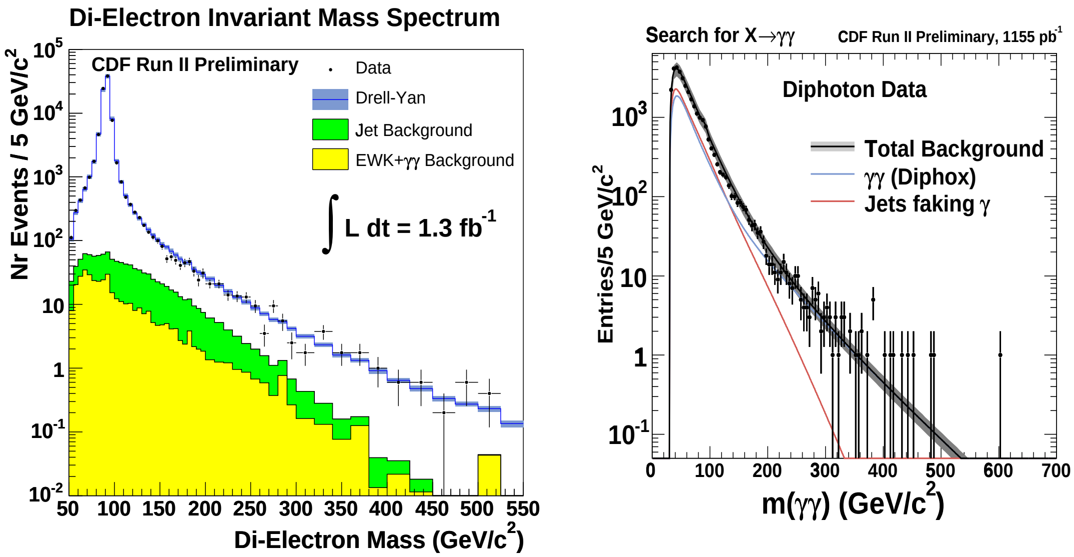

FIGURE 24. Invariant mass distribution observed in dielectron (left) and diphoton (right) events, and expected SM distribution.

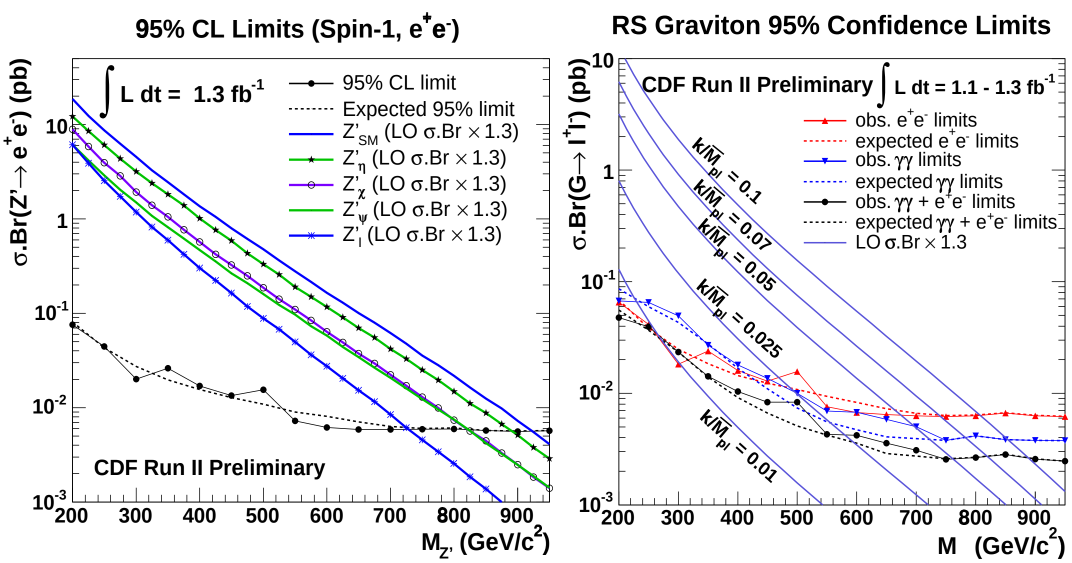

FIGURE 25. The 95% CL upper limits on cross section times BR as a function of $M_{Z'}$ for the dielectron final states (left) and as a function of M_G for ee, $\gamma\gamma$, and combined $ee+\gamma\gamma$ final states (right).

Increasingly sophisticated analysis techniques and improved detector understanding and performance, together with increasing data samples, allow to probe some of the smallest cross sections ever measured at hadron colliders. Evidence for processes such as WZ, ZZ and single top production has been found. The study of top quark is unique to the Tevatron. CDF has performed the most precise single determination of its mass, and measured its production and decay properties. CDF is a hadron collider experiment which has produced several B physics results which are competitive with dedicated B

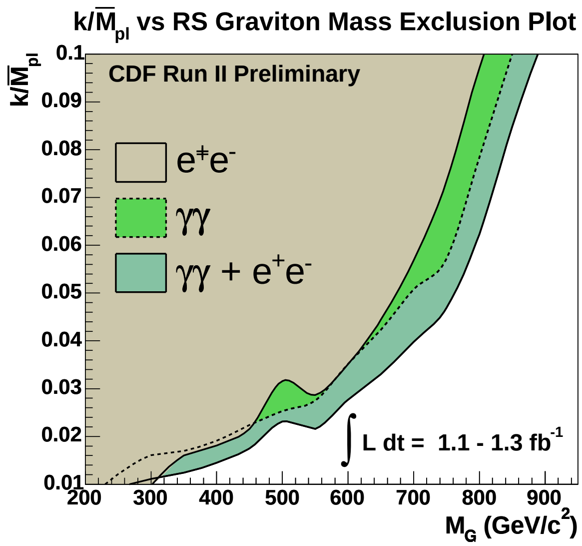

FIGURE 26. The 95% CL excluded region on the $k/M_{\rm Plank}$-M_G plane.

factories, and some of the most precise electroweak measurements to date, bringing SM tests to a level of precision similar or better than electron-positron colliders. Continuous improvements in the expected sensitivity of searches for Higgs and for physics beyond the SM allow significant exclusion or reach on many different models. In particular, CDF (and D0) might have something interesting to say about the Higgs if enough luminosity is recorded during the next two years, making the search for Higgs a top priority.

REFERENCES

1. R. Blair *et al.* (CDF Collaboration), *The CDF-II detector Technical Design Report*, FERMILAB-PUB-96-390-E.
   D. Acosta *et al.* (CDF Collaboration), Tech. Rep. FERMILAB-PUB-04/440-E (2004).
2. G. C. Blazey *et al.*, *QCD and weak boson physics in Run II*, pp. 47-77, preprint hep-ex/0005012.
3. W. Ashmanskas *et al.*, *Nucl. Instr. Meth. Phys. Res. Sect. A* **518**, 532 (2004).
4. B. W. Harris *et al.*, *Phys. Rev. D* **66**, 054024 (2002); Z. Sullivan, *Phys. Rev. D* **70**, 114012 (2004).
5. M. Carena, S. Heinemeyer, C.E.M. Wagner and G. Weiglein, preprint hep-ph/9912223 (1999).
6. N. Arkeni-Hamed, S. Dimopoulos and G. Dvali, *Phys. Lett.* **B429** (1998).
7. J.L. Hewett and T.G. Rizzo, *Phys. Rept.* **183**, 193 (1989).
   D. London and J.L. Rosner, *Phys. Rev. D* **34**, 1530 (1986).
8. L. Randall and R. Sundrum, *Phys. Rev. Lett.* **83**, 3370 (1999).